Supporting information

Size and Charge Dual-Transformable Mesoporous Nanoassemblies for Enhanced Tumor Delivery and Penetration

*Liang Chen,[a] Tiancong Zhao,[a] Mengyao Zhao,[a] Wenxing Wang,[a] Caixia Sun,[a] Lu Liu,[a] Qin Li,[b] Fan Zhang,[a] Dongyuan Zhao,[a] Xiaomin Li,[a]**

Dr. L. Chen, Mr. T. C. Zhao, Mrs. M. Y. Zhao, Dr. W. X. Wang, Mrs. C. X. Sun, Dr. L. Liu, Prof. Dr. F. Zhang, Prof. Dr. D. Y. Zhao, Prof. Dr. X. M. Li
Department of Chemistry and Laboratory of Advanced Materials, State Key Laboratory of Molecular Engineering of Polymers, Collaborative Innovation Center of Chemistry for Energy Materials (2011-*i*ChEM), Fudan University, Shanghai 200433, P. R. China.
E-mail: lixm@fudan.edu.cn

Prof. Dr. Q. Li

Queensland Micro- and Nanotechnology Centre, & School of Engineering & Built Environment, Griffith University, Nathan, QLD 4111, Australia.

Materials

Hexadecyltrimethylammonium bromide (CTAB), tetraethyl orthosilicate (TEOS), 3-aminopropyltriethoxysilane (APTES), 1-octadecene (ODE, 90 %), oleic acid (OA, 90 %) and polyethylenimine (PEI) were purchased from Sigma-Aldrich Trading Co., Ltd. Triethanolamine (TEA), 2, 3-dimethylmaleic anhydride (99.5%), Rose bengal (RB) and 1, 3-Diphenylisobenzofuran (DPBF) were provided by Aladdin Chemistry, Co., Ltd. Gadolinium (III) chloride anhydrous ($GdCl_3$, 99.99 %), yttrium (III) chloride anhydrous (YCl_3, 99.9 %), ytterbium (III) chloride anhydrous ($YbCl_3$, 99.9 %), erbium (III) chloride anhydrous ($ErCl_3$, 99.9 %), neodymium (III) chloride hexahydrate ($NdCl_3$, 99.9 %) and sodium trifluoroacetate (Na-TFA, 98 %) were purchased from Sigma-Aldrich Trading Co., Ltd. Doxorubicin hydrochloride was obtained from Huafeng United Technology Co., Ltd.. Fetal bovine serum (FBS), penicillin-streptomycin, trypsin, and Roswell Park Memorial Institute (RPMI) 1640 medium were provided from Gibco Life Technologies Co. Paraformaldehyde was purchased from Beijing Dingguo Changsheng Biotechnology Co., Ltd. 4′,6-Diamidino-2-phenylindole (DAPI) was purchased from Bestbio. All other regents were of analytical grade and commercially available. Deionized (DI) water was used throughout the experiments.

Synthesis of Carboxyl Functionalized MSNs

Pure MSNs: Typically, 3.00 g CTAB and 120 μL TEA was dissolved in 60.0 mL water and heated to 60 °C for 1 h. Then 16.0 mL cyclohexane and 4.0 mL TEOS were mixed and slowly added onto the upper layer of water phase. The mixture was further stirred at 200 rpm for 24 h. The products were isolated by high-speed centrifugation and washed several times with ethanol. To remove the surfactant of CTAB, the MSNs was dispersed in HCl-ethanol solution (10.0 wt%) and refluxed for 12 h, the process was repeated several times.

Amino functionalized MSNs: The obtained MSNs were reacted with APTES for surface functionalization of amino group. 0.10 g MSNs and 100 μL APTES were dispersed in 50.0 mL anhydrous ethanol and refluxed at 80 °C for 12 h. The resultant MSNs-NH_2 were collected by centrifugation and washed for a few times.

Carboxyl functionalized MSNs: The MSNs-NH_2 were dispersed in DMSO under ultrasonication. 50.0 mg 4-formylbenzoic acid were added, and the mixture was stirred at 50 °C for 4 h. Then, the benzaldehyde−linked MSNs-COOH was collected by centrifugation and washed with anhydrous

ethanol twice.

Synthesis of $NaGdF_4$:Yb/Er@$NaYF_4$@$NaGdF_4$:5%Nd@$NaYF_4$ U/DCNPs

Synthesis of $NaGdF_4$:Yb/Er nanocrystals*:* Hexagonal phase $NaGdF_4$:20%Yb/2%Er nanocrystals were synthesized according to a previously reported thermolysis method[1]. Typically, $GdCl_3$ (0.78 mmol), $YbCl_3$ (0.20 mmol), $ErCl_3$ (0.02 mmol), OA (6.0 mL) and ODE (15.0 mL) were mixed together and heated to 140 °C under vacuum until a clear solution formed. After that, the solution was cooled down to room temperature. Then, a methanol solution (10.0 mL) of ammonium fluoride (4.00 mmol) and sodium hydroxide (2.50 mmol) was added and stirred for 1 h at 50 °C. The mixture was then heated to 70 °C and maintained under vacuum for half an hour to remove the methanol. Afterward, the solution was heated to 270 °C (~ 10 °C/min) and maintained for 90 min under a gentle argon flow. Then, the solution was cool down to room temperature and the nanocrystals were centrifuged and washed twice with ethanol. The nanocrystals were finally dispersed in 10.0 mL of cyclohexane for further use.

Y-OA (0.10 M), Gd-OA (0.10 M) and Nd-OA (0.1 M) shell precursor: 2.50 mmol of YCl_3 (or $GdCl_3$ or $NdCl_3$), 10.0 mL of OA, and 15.0 mL of ODE were mixed in a round-bottom flask and heated at 140 °C under vacuum with magnetic stirring for 30 min to remove residual water and oxygen. Then the colorless Y-OA (Gd-OA or Nd-OA) precursor solution (0.10 M) was obtained.

Na-TFA-OA (0.40 M) shell precursor: A mixture of Na-TFA (4.00 mmol) and OA (10.0 mL) was loaded in a container at room temperature under vacuum with magnetic stirring to remove residual water and oxygen. Then the colorless Na-TFA-OA precursor solution (0.40 M) was obtained.

Synthesis of core@shell structured nanocrystals: The core@shell nanoparticles were fabricated by using the one-pot successive layer-by-layer (SLBL) protocol, which was developed by our group[2]. 2.5 mL of the purified $NaGdF_4$:Yb/Er core nanoparticles solution (~ 0.25 mmol) were mixed with 4.0 mL of OA and 6.0 mL of ODE. The flask was pumped down at 70 °C for 30 min to remove cyclohexane. After that, the system was switched to Ar flow and the reaction mixture was further heated to 280 °C at a rate of ~ 20 °C/min. Then pairs of Y-OA (0.10 M, 1.0 mL) and Na-TFA-OA (0.40 M, 0.50 mL) precursors were alternately introduced by dropwise addition at 280 °C and the time interval between each injection was 15 min. Finally, the obtained $NaGdF_4$:Yb/Er@$NaYF_4$ core@shell nanoparticles were precipitated and washed in the same way

as the core nanoparticles, and dispersed in cyclohexane.

The growth of $NaGdF_4$:5%Nd shell onto $NaGdF_4$:Yb/Er@$NaYF_4$ was proceeded with the same SLBL protocol, in which the Gd-Nd-OA (a mixture of Gd-OA and Nd-OA with the ratio of 0.95 : 0.05) and Na-TFA-OA (0.40 M) shell precursors were used to grow the $NaGdF_4$:5%Nd layer. For the outer most $NaYF_4$ inert layer, the Y-OA (0.10 M) precursor was used. The obtained $NaGdF_4$:Yb/Er@$NaYF_4$@$NaGdF_4$:Nd@$NaYF_4$ U/DCNPs were washed with ethanol and re-dispersed in 5.0 mL cyclohexane.

Surface Modification of U/DCNPs with PEI

First, the oleic acid-capped U/DCNPs (2.0 mL in cyclohexane) were mixed with 10.0 mL of ethanol solution of HCl (2 %). The mixture was subjected to ultrasonic treatment for 10 min. Then the ligand-free U/DCNPs were collected by high-speed centrifugation and re-dispersed in 10.0 mL DI water. 1.0 mL PEI solution (20 mg/mL) was added dropwise and stirred for 30 min. Then PEI modified U/DCNPs were collected and washed with water.

Fabrication of MSN@U/DCNPs Nanoassemblies

The PEI modified U/DCNPs was covalently conjugated onto large MSNs. Briefly, 50.0 mg carboxyl group functionalized MSNs was dispersed in 20 mL of DI water and the pH was adjusted above 8. Then, 10.0 mL of PEI modified U/DCNPs was added and maintained for 12 h. After that, the nanocomposites of MSN@U/DCNPs-PEI were obtained and washed by water (pH >8).

The MSN@U/DCNPs were further capped with PAH-DMMA-PEG, which were synthesized with the same procedure of previous publication.[3] Typically, MSN@U/DCNPs were dispersed in DI water (pH >8) at concentration of 2 mg/mL. Then 20 mg of PAH-DMMA-PEG was added, and the mixture was stirred for 2 h to obtain the PAH-DMMA-PEG capped MSN@U/DCNPs nanoassemblies.

Characterization

The morphology of prepared nanoparticles were observed by transmission electron microscopy (TEM) under accelerated voltage of 200 kV (FEI, American). Scanning electron microscopy (SEM) images were captured using field emission scanning electron microscopy (FESEM, Hitachi S-4800, Japan). X-ray diffractions (XRD) of samples were recorded on a D/max-2550 PC X-ray diffractometer (XRD; Rigaku, Japan). UV–vis–NIR absorption spectra were measured on a Shimadz spectrophotometer (UV-3150) (Japan). Size distribution and Zeta potential of the samples

were recorded by using Zetasizer Nano ZS apparatus (Malvern, UK). The concentrations of Gd element were analyzed by a Leeman Prodigy inductively coupled plasma-atomic emission spectroscopy (ICP-AES) system (Hudson, NH03051, USA). Fourier transform infrared (FTIR) spectra were recorded using a NICOLET MX-1E FTIR spectrometer. NMR spectra were performed using Bruker AV 300 NMR system, and chemical shifts (δ, ppm) were recorded by using internal reference tetramethylsilane (TMS).

In Vitro Cytotoxicity Evaluation

Murine breast cancer cell line (4T1 cells) and mouse leukemic monocyte macrophage cell line (RAW 264.7 cells) were purchased from cell bank of Chinese academy of science (Shanghai, China). The cells were cultured in standard Roswell Park Memorial Institute (RPMI) 1640 medium supplemented with 10% (v/v) FBS, 100 mg mL^{-1} streptomycin and 100 U mL^{-1} penicillin at 37 °C in a humidified incubator with 5% CO_2.

The cytotoxicity of the prepared MSN@U/DCNPs nanoassemblies was assessed using standard CCK-8 assay. 4T1 or RAW 264.7 cells were seeded in 96-well plates (10^4 cells/well) for 24 h. After that, the cells were incubated with fresh medium containing different concentrations of MSN@U/DCNPs (400, 200, 100, 50, 25, 12.5, 6.25 μg/mL) for another 24 h. Then, the medium was discarded and the cells were slightly washed by PBS, followed by the standard CCK-8 protocol according to the manufacturer's instruments. Cells treated with pure medium without MSN@U/DCNPs was used as control group. Four parallel experiments were performed for each group.

In Vitro Cell Uptake

The cell uptake of MSN@U/DCNPs nanoassemblies was first investigated by confocal laser scanning microscopy (CLSM, Olympus FV900). 4T1 cells were seeded in glass-bottom culture dish (3.0×10^5 cells per dish) and incubated with MSN@U/DCNPs at two different pH conditions (7.4 and 6.5) for 4 h. Subsequently, the cells were slightly rinsed with PBS, fixed with 4% paraformaldehyde, and stained with DAPI for direct observation.

Meanwhile, the intracellular uptake of MSN@U/DCNPs by 4T1 cells was also quantified by measuring Gd content. After being incubated with MSN@U/DCNPs at different pH conditions for 4 h, the cells were repeatedly washed with PBS, trypsinized, and lyophilized. Then the samples were fully dissolved in HNO_3 aqueous solutions and diluted with DI water. Finally, the transparent

solution can be obtained and used for quantitative analysis of Gd concentration by ICP-AES.

Multi-Cells Spheroids (MCSs) Experiments

The deep tumor penetration capacity of prepared nanoassemblies was evaluated by simulated MCSs experiment. To establish the MCSs, 4T1 cells were detached from culture flask and seeded in customized 96-well plate with low adhesion bottom at a density of 4.0×10^5 cells per well. 50.0 uL of matrix gel was added into each well. The cells were further incubated at 37 °C for 2 weeks to allow the sufficient growth of MCSs. The culture medium was half replaced with fresh medium every two days. After the MCSs reached appropriate size, the MCSs were incubated with MSN@U/DCNPs (200 μg/mL) at two pH conditions (7.4 and 6.5) for 6 h. Then, the medium was carefully removed, and the MCSs was carefully rinsed with PBS for CLSM observation. The position of the nanoassemblies in MCSs was located by the green upconversion fluorescence of U/DCNPs under the 980 nm laser irradiation. The images at various depth of MCSs was captured and the line scanning analysis of fluorescence intensity was performed on CLSM software.

In Vitro ROS Detection

First, 5.0 mg of RB was added into the aqueous dispersion of prepared U/DCNPs-PEI (10 mM of U/DCNPs). The mixture was stirred overnight, and the RB photosensitizers were absorbed onto the surface of U/DCNPs-PEI by physical adsorption. The RB loaded U/DCNPs-PEI were washed and separated by centrifugation. Finally, the RB loaded U/DCNPs-PEI were also conjugated onto MSNs by the same procedure mentioned above.

To evaluate the ROS generation ability, 2.0 mL of MSN@U/DCNPs-RB in DMSO was mixed with 50 uL of DPBF solution (3 mM). The mixture was then irradiated by 980 nm laser (2 W/cm^2) for different time periods. In the mixture, the absorption of DPBF at 420 nm is indicator of the generation of ROS, which can be determined by UV-vis spectrophotometer.

For the intracellular detection of ROS, 4T1 cells were first incubated with MSN@U/DCNPs-RB at different pH conditions (7.4 and 6.5) for 4 h. Then the cells were washed with PBS and further cultured in fresh medium containing DCFH-DA probe for 30 min. Thereafter, the cells were exposed to 980 nm laser for 20 min and washed for the CLSM observation. Moreover, the quantitative analysis of the fluorescence signal from the cells can also be determined by flow cytometry.

Evaluation of In Vitro Therapeutic Efficacy

4T1 cells were seeded on a 96-well plate at a density of 10^4 cells/well. After that, the cells were incubated with DOX-MSN@U/DCNPs, MSN@U/DCNPs-RB and DOX-MSN@U/DCNPs-RB at different pH conditions (7.4 and 6.5) for 4 h. Subsequently, the cells were slightly rinsed with fresh medium. The groups of RB-MSN@U/DCNPs and DOX-MSN@U/DCNPs-RB were exposed to 980 nm laser for 20 min. Then, cells were rinsed with PBS for several times and incubated for another 20 h. Finally, the standard CCK-8 assay was conducted to evaluate the cell viability of each group. For visualizing the killing effect, the cells were also stained with Calcein-AM/PI after different treatments and observed by CLSM.

In Vivo Bio-Distribution

All animal experiments were conducted complying with guidelines of Institutional Animal Care and Use Committee (IACUC). For in vivo experiment, 4~6 week-old Female Balb/c mice were commercially supplied by Slac Laboratory Animal Co. Ltd. (Shanghai, China). 4T1 cells were detached from culture flask and suspended in FBS. Then 4×10^6 cells were subcutaneously injected into the right back leg of mice. When the tumors reached 4~6 mm in diameter, the tumor-bearing mice were intravenously injected with the MSN@U/DCNPs nanoassemblies (25 mg/kg). Under the excitation of 808 nm, the downconversion NIR-II fluorescent signal from nanoassemblies can be detected by the NIR camera. In order to avoid the interaction from the signal of non-interested area, a screener with only the tumor area exposed was used. The PEI modified free U/DCNPs were used as the control group. The mice were sacrificed at 24 h post injection, and the major organs including heart, liver, spleen, lung and kidney were weighted and digested by *aqua regia* (Caution! Aqua regia produces hazardous gases and will explode upon contact with organics). The samples were subjected to ICP-AES for measuring Gd concentration.

The pharmacokinetics of MSN@U/DCNPs and PEI modified free U/DCNPs were also investigated by monitoring the Gd concentration in the blood. Concretely, MSN@U/DCNPs and free U/DCNPs were intravenously injected into mice. Thereafter, the blood were taken from the eyeballs of the mice at different time points post injection (1 min, 10 min, 30 min, 1 h, 2 h, 4 h and 8 h). The obtained samples were also digested in aqua regia and measured by ICP-AES. After 24 h, the mice were euthanized and the major organs were excreted, fixed and used for hematoxylin-eosin (H&E) staining.

In Vivo Anti-Tumor Effect

The tumor-bearing mice were randomly divided into four groups (n = 4 for each group): control group, DOX-MSN@U/DCNPs, MSN@U/DCNPs-RB + NIR laser, and DOX-MSN@U/DCNPs-RB + NIR laser. The tumor-bearing mice were anesthetized with an intraperitoneal injection of pentobarbital sodium. Then, the samples were intravenously injected, and 980 nm laser irradiation (2 W/cm^2, 20 min) was performed at 6 h post-injection. To avoid the thermal effect of 980-nm laser, the irradiation for PDT is intermittently performed with 2 min interval after each minute irradiation (**Figure S24**). The total irradiation time in each PDT treatment is 20 min. The treatments were conducted at days 1, 3 and 5. After that, the tumor sizes were measured by digital caliper. The body weights of experimental mice were monitored during treatments. Additionally, the tumor tissue of each group after the treatments were excised for H&E and TUNEL staining.

Statistical Analysis

At least three independent groups were performed throughout experiment. Significant difference between different groups was analyzed by one-way analysis of variance (ANOVA) and Scheffe's post hoc test. The criterion was expressed as *P < 0.05 and **P < 0.01.

References

[1] X. M. Li, R. Wang, F. Zhang, D. Y. Zhao, *Nano Lett* **2014**, *14*, 3634.

[2] X. M. Li, D. K. Shen, J. P. Yang, C. Yao, R. C. Che, F. Zhang, D. Y. Zhao, *Chem Mater* **2013**, *25*, 106.

[3] T. Feng, X. Z. Ai, G. H. An, P. P. Yang, Y. L. Zhao, *ACS Nano* **2016**, *10*, 4410.

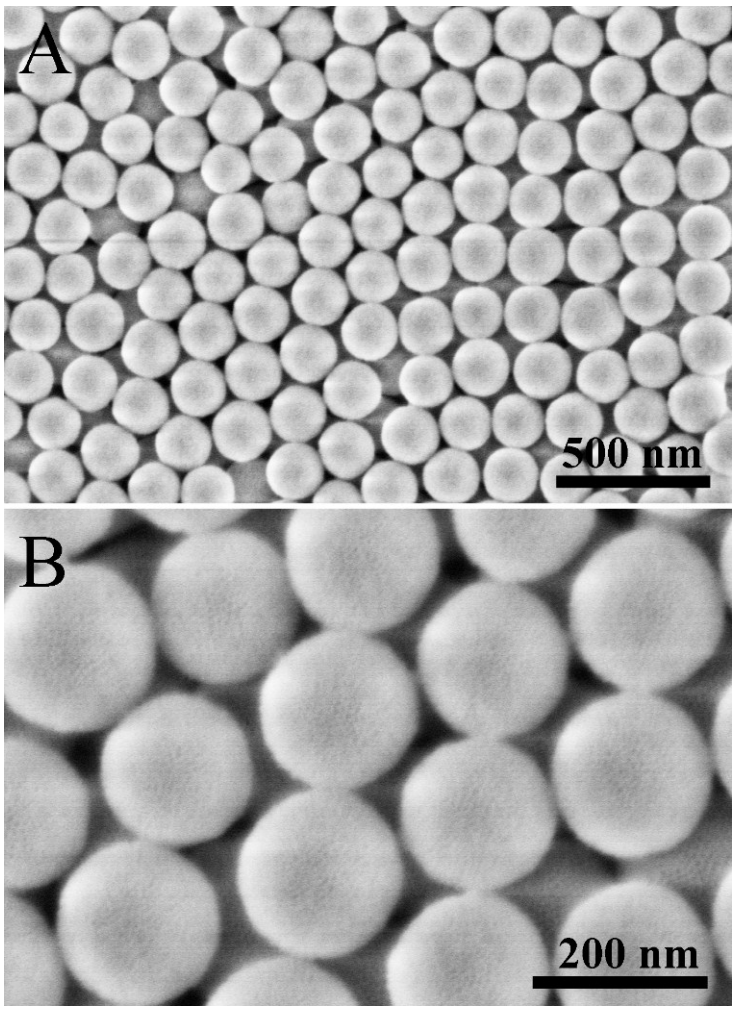

Figure S1. SEM images of as-prepared MSNs with (A) low and (B) high magnifications. It can be seen that the obtained MSNs are very uniform with the diameter of ~180 nm. The open mesoporous channels can be clearly observed.

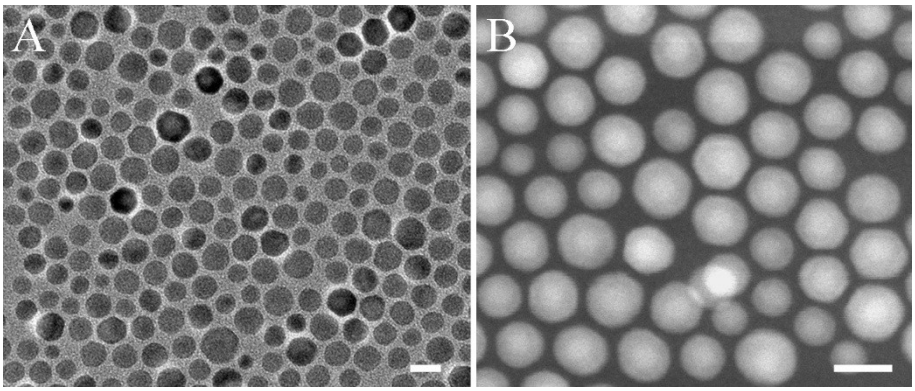

Figure S2. TEM (A) and HAADF-STEM (B) images of as-prepared U/DCNPs, scale bar in A and B was 20 nm. It can be seen that the as-prepared U/DCNPs show discernible contrast for the core@multi-shell structure with an average diameter of approximately 18 nm.

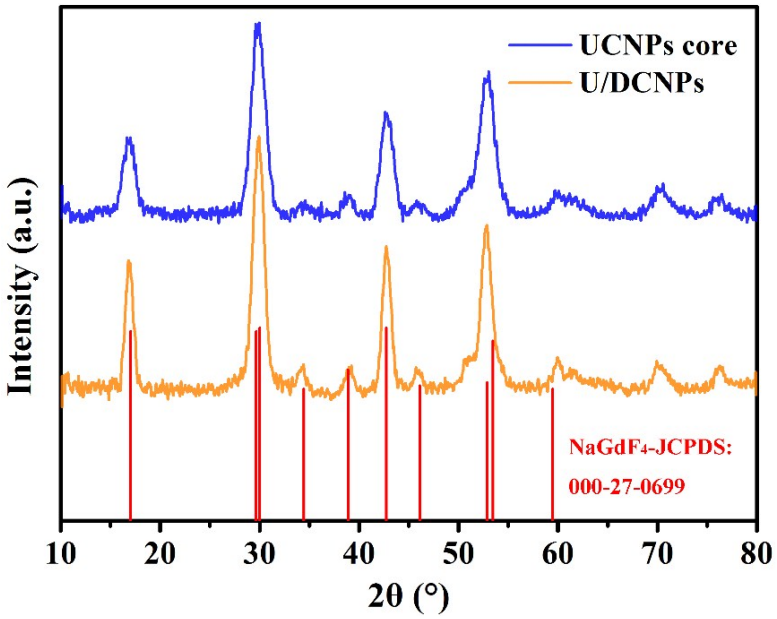

Figure S3. XRD patterns of the $NaGdF_4$:Yb/Er UCNPs, multi-shelled $NaGdF_4$:Yb/Er@$NaYF_4$@$NaGdF_4$:Nd@$NaYF_4$ U/DCNPs and the corresponding JCPDS cards, indicating the highly crystalline hexagonal phase without impurity phases.

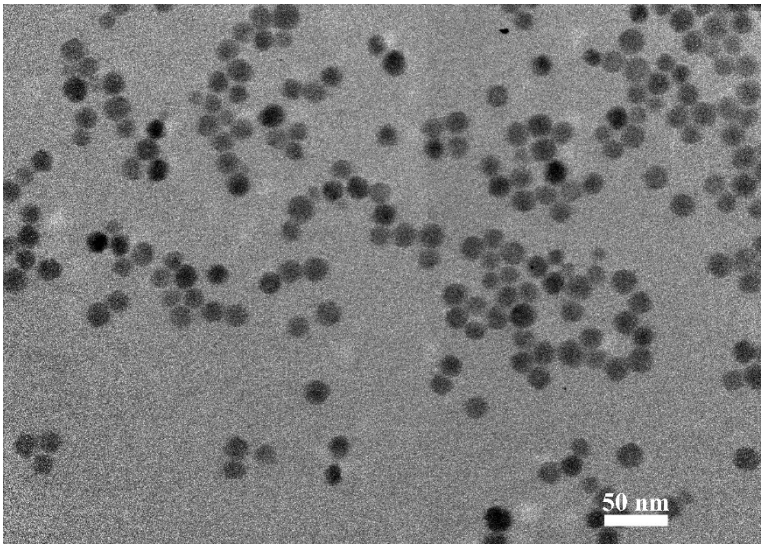

Figure S4. TEM image of the PEI modified U/DCNPs. It can be seen that the monodispersity of the U/DCNPs is maintained well after the surface modification of PEI.

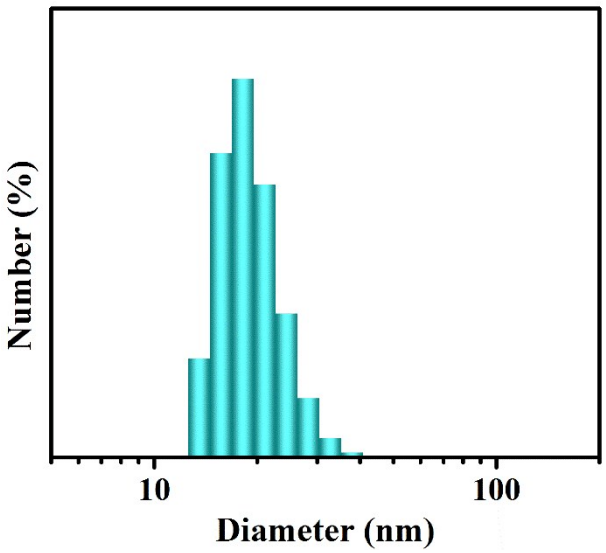

Figure S5. The size distribution of UCNPs-PEI measured by DLS. It can be seen that the diameter of the PEI modified U/DCNPs is around 20 nm, and the size distribution is very narrow.

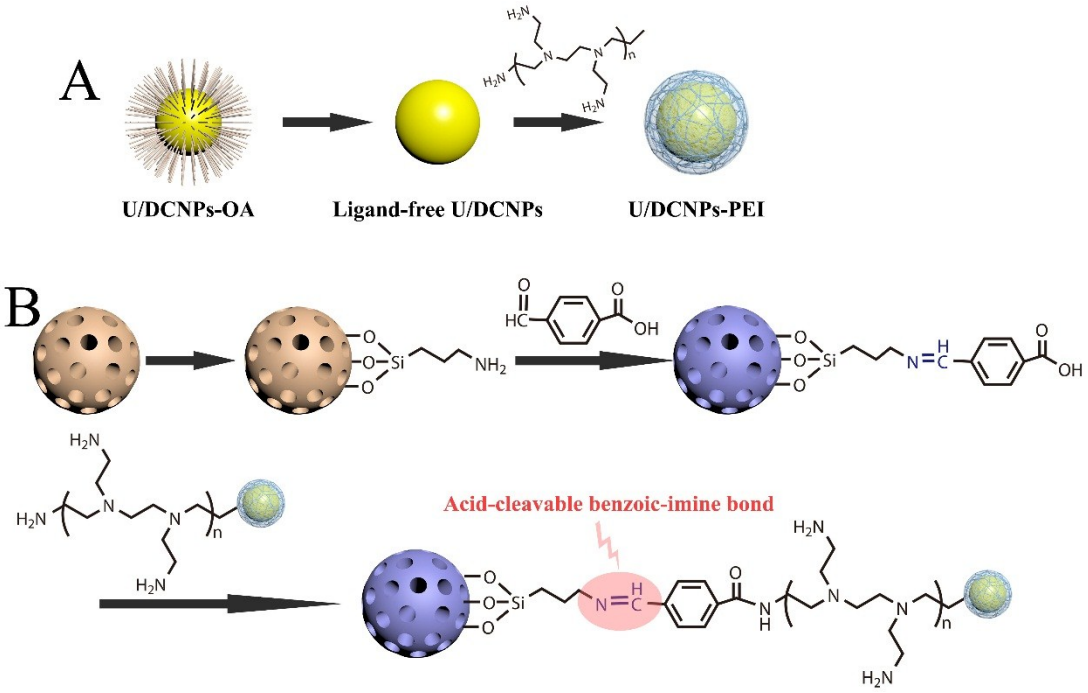

Figure S6. Schematic illustration of the fabrication process of (A) PEI modified U/DCNPs and (B) conjugation between U/DCNPs and MSN. The oleic acid (OA) capped U/DCNPs are treated by ethanol-HCl solution to form the ligand-free U/DCNPs. Then PEI can easily attach on the U/DCNPs according to the coordination between the amino groups and rare-earth ions. For designing of acid-labile linker between MSN and U/DCNPs, 4-formylbenzoic acid is introduced. The MSNs are first functionalized with amino groups, and then conjugate with 4-formylbenzoic acid to form the acid cleavable benzoic-imine bond. The exposed carboxyl groups on the surface of MSNs can be used for the conjugation of PEI modified U/DCNPs.

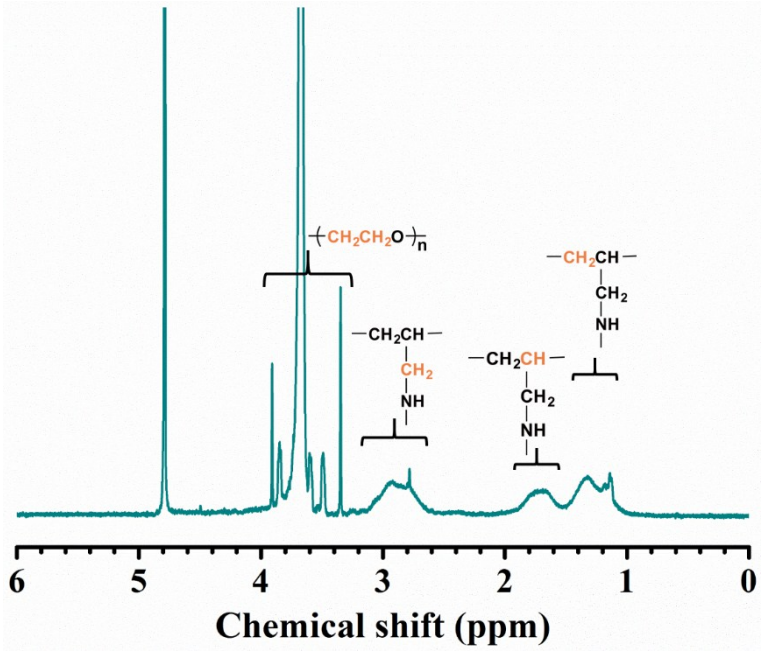

Figure S7. ^{1}H NMR (300 MHz, D_2O) spectrum of PAH-PEG.

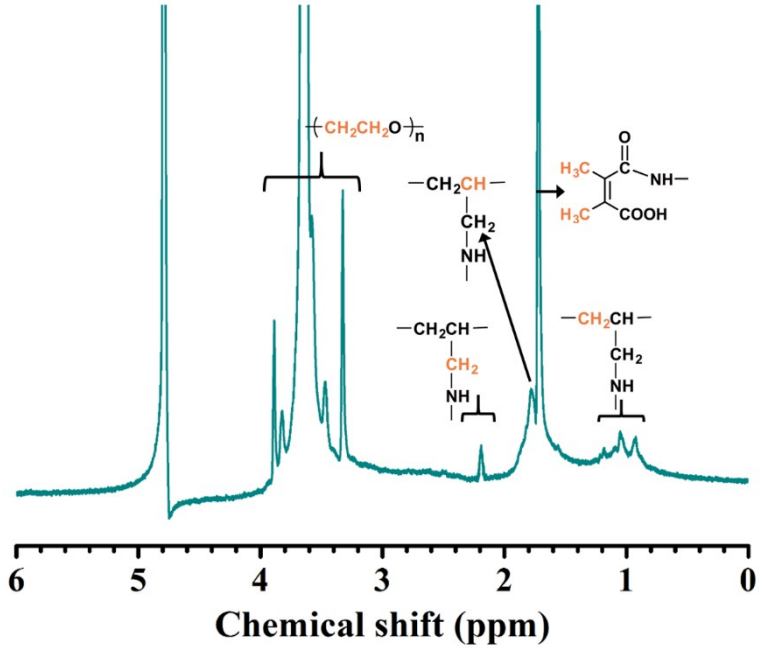

Figure S8. ^{1}H NMR (300 MHz, D_2O) spectrum of PAH-DMMA-PEG.

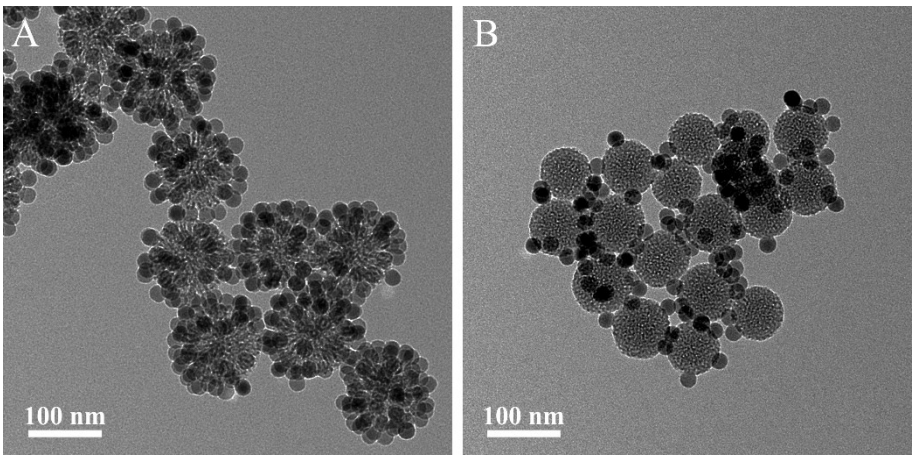

Figure S9. TEM images of nanoassemblies prepared with (A) 100-nm and (B) 80-nm MSNs. The results indicating that the U/DCNPs can also be conjugated onto smaller MSNs. However, upon the size of MSNs reduced to 80 nm, only a few U/DCNPs is attached onto MSNs, indicating the crosslinking efficiency between the U/DCNPs and MSNs is decreased. The decreased efficiency is probably due to the variation of curvature of the MSNs surface.

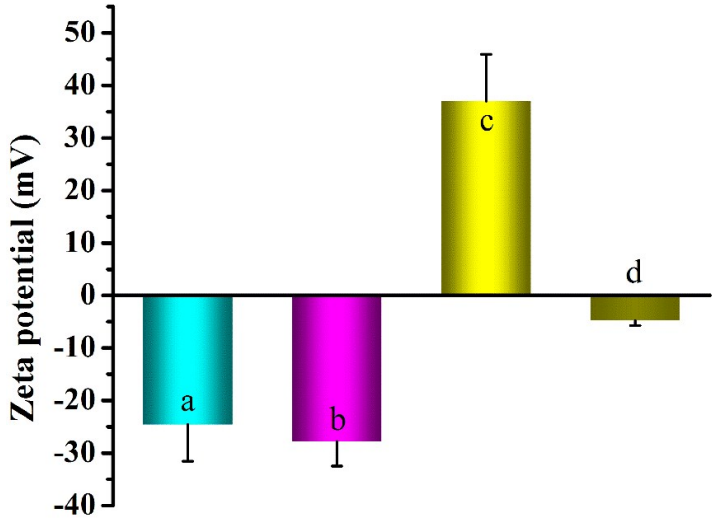

Figure S10. Zeta potential of different samples a) bare MSNs, b) 4-formylbenzoic acid modified MSNs, c) U/DCNPs-PEI conjugated MSNs and d) PAH-DMMA-PEG capped nanoassemblies. It can be seen that the surface charge of the bare MSNs is negative, which is maintained after the surface modification of 4-formylbenzoic acid. In comparison, the surface charge transfer to positive after the conjugation of U/DCNPs-PEI, because of the strong positive electricity of the PEI. After capping with the outer most pH-responsive PAH-DMMA-PEG, the nanoassemblies exhibit slight negative charge, which is crucial for the prolonged blood circulation.

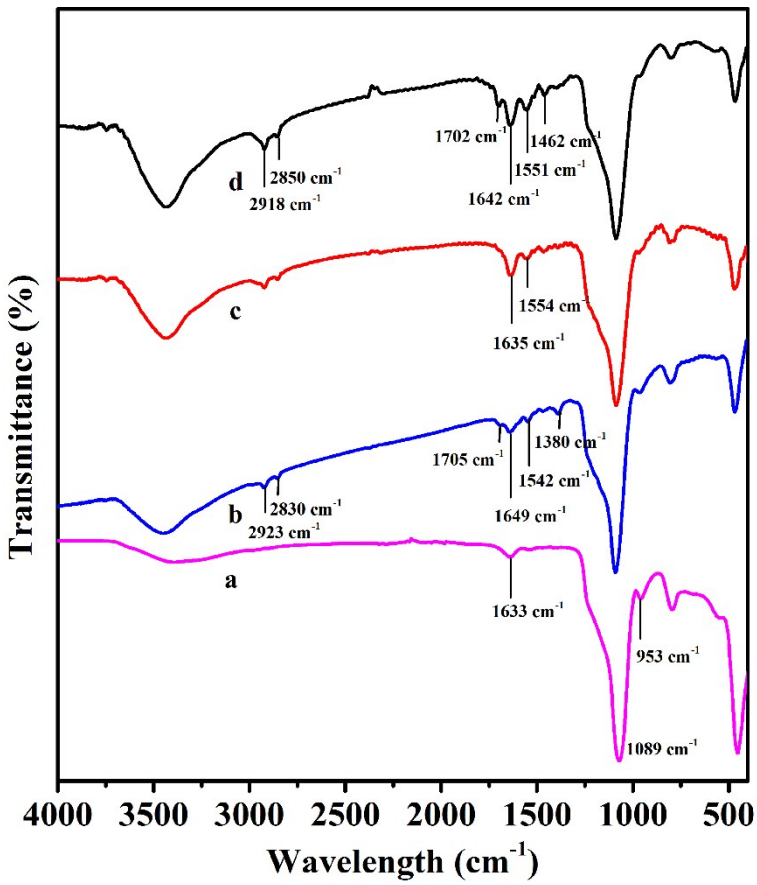

Figure S11. FTIR spectra of (a) MSNs-NH_2, (b) 4-formylbenzoic acid functionalized MSNs, (c) MSN@U/DCNPs-PEI, and (d) PAH-DMMA-PEG capped MSN@U/DCNPs nanoassemblies, respectively. MSNs-NH_2 displays characteristic peaks at 1089 cm^{-1} and 953 cm^{-1}, which can be ascribed to the asymmetric stretching vibration of Si-O-Si bridges and stretching vibration of Si–O bonds. The peak at 1633 cm^{-1} can be assigned to the stretching vibration of amide I band of -NH_2 group. After conjugating with 4-formylbenzoic acid, the distinct absorption peaks at 1649 cm^{-1} and 1542 cm^{-1} can be assigned to the stretch vibration of C=N, indicating the formation of Schiff base. The peaks at 2923 cm^{-1} and 2830 cm^{-1} is attributed to the stretching vibration of C–H bond. Moreover, the absorption peak at 1380 cm^{-1} is the stretching vibration of C–O bond, and the presence of peak at 1705 cm^{-1} is the typical absorption

of carboxyl groups in 4-formylbenzoic acid, which demonstrates that the successful modification of 4-formaylbenzoic acid onto MSNs. In addition, the absorption of carboxyl groups at 1705 cm^{-1} disappear after conjugation of U/DCNPs-PEI, implying that the surface carboxyl groups on the MSNs are totally participated in the amidation reaction. Last, the FTIR spectrum of PAH-DMMA-PEG capped MSN@U/DCNPs nanoassemblies shows the typical peaks at 1670 cm^{-1}, 1626 cm^{-1}, and 1562 cm^{-1}, which can be attributed to functional groups of amide and carboxylic acid in β-carboxylic amide. Overall, the results of FTIR confirm that the nanoassemblies are successfully constructed.

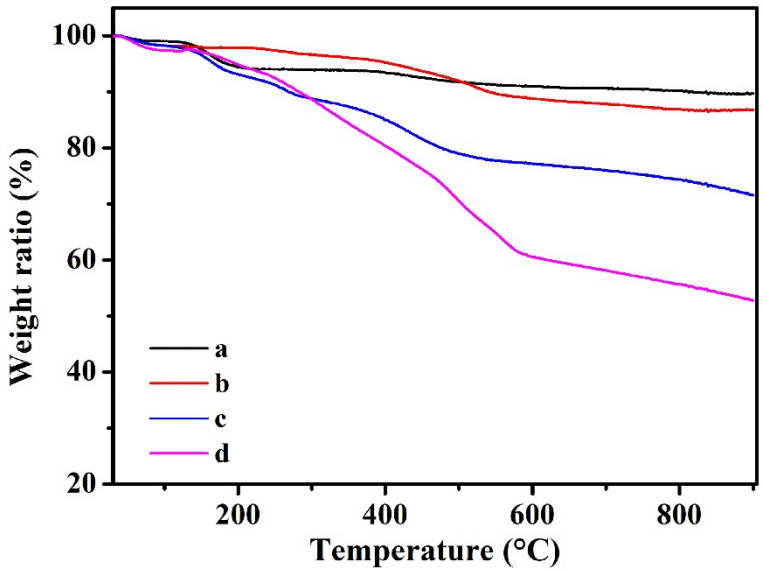

Figure S12. Thermogravimetric analysis of (a) MSNs-NH_2, (b) 4-formylbenzoic acid functionalized MSNs, (c) MSN@U/DCNPs-PEI, and (d) PAH-DMMA-PEG capped MSN@U/DCNPs nanoassemblies, respectively. The weight loss of MSNs-NH_2 is calculated to be 10.32 %, while it increased to 14.02 % after the conjugation of 4-formylbenzoic acid. Further, the value reaches to 28.5 % and 47.31 % for MSN@U/DCNPs-PEI and the nanoassemblies, respectively. The results suggest that the content of organic compounds is gradually increased in the preparation process of the final nanoassemblies, confirming the successful construction of the designed nanoassemblies.

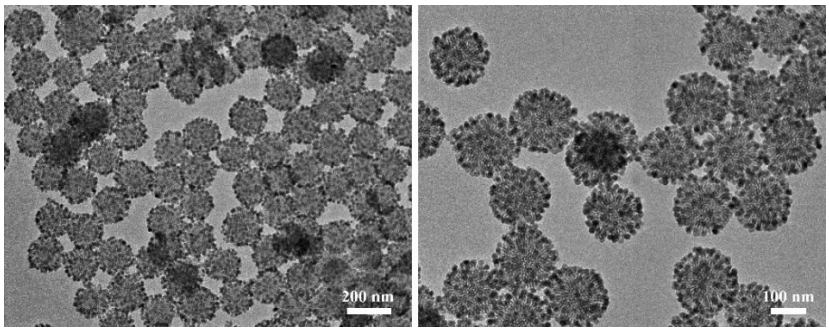

Figure S13. TEM images with different magnifications of MSN@U/DCNPs nanoassemblies after 30 min ultrasonic treatments. The core@satellites structure of the nanoassemblies are maintained very well, indicating the conjugation between MSNs and U/DCNPs is very stable.

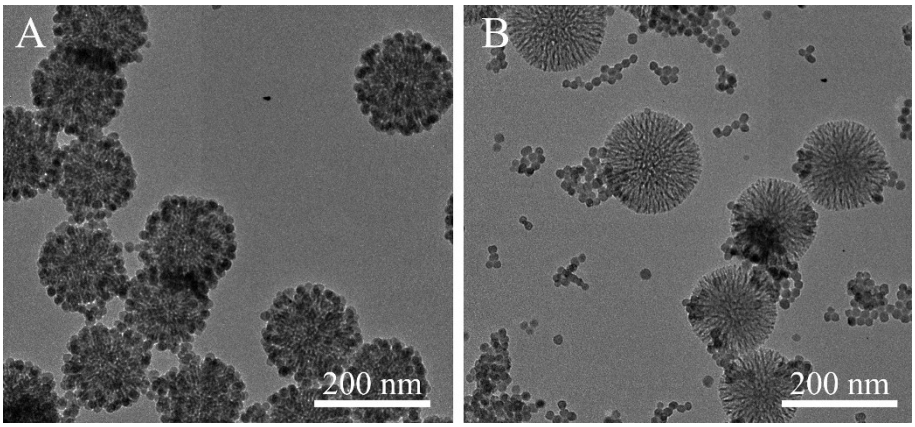

Figure S14. TEM images of nanoassemblies dispersed in (A) cell culture medium and (B) incubated in cell culture medium at pH 6.5 for 6 h. It can be seen that the nanoassemblies exhibits good dispersity in cell culture medium without obvious aggregation. Meanwhile, the dissociation of nanoassemblies is observed under weak acidic condition.

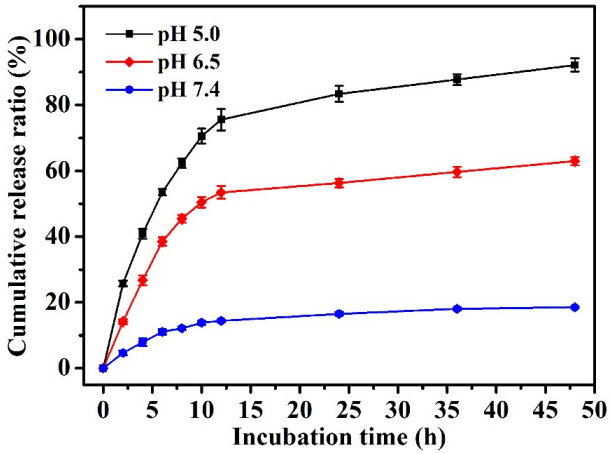

Figure S15. The cumulative releasing amount of DOX from DOX-MSN@U/DCNPs nanoassemblies at different pH. Because of the attachment of U/DCNPs and charge-reversible polymer onto MSNs surface, the mesopores of MSNs are partially blocked, and less than 20 % of DOX can be released within 48 h under physiological condition. In comparison, the drug release at acidic pH was much faster than that at physiological pH. At pH 5.0 and 6.5, the cumulative DOX release ratio reached over 80 % and 60 % in 48 h, respectively.

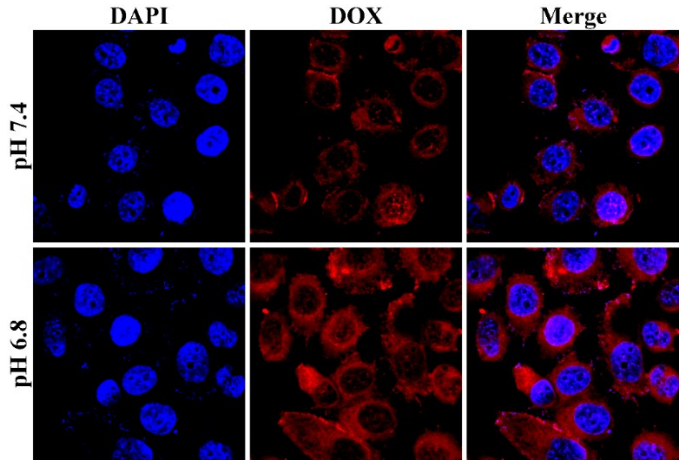

Figure S16. The confocal laser scanning microscopy images of 4T1 cells exposed to DOX-MSN@U/DCNPs nanoassemblies with benzoic-imine linker between the MSN and U/DCNPs. After incubation for 4 h, the red fluorescence of DOX in the cells at pH 6.5 is much brighter than that of at pH 7.4, implying that much faster intracellular delivery of DOX under acidic condition.

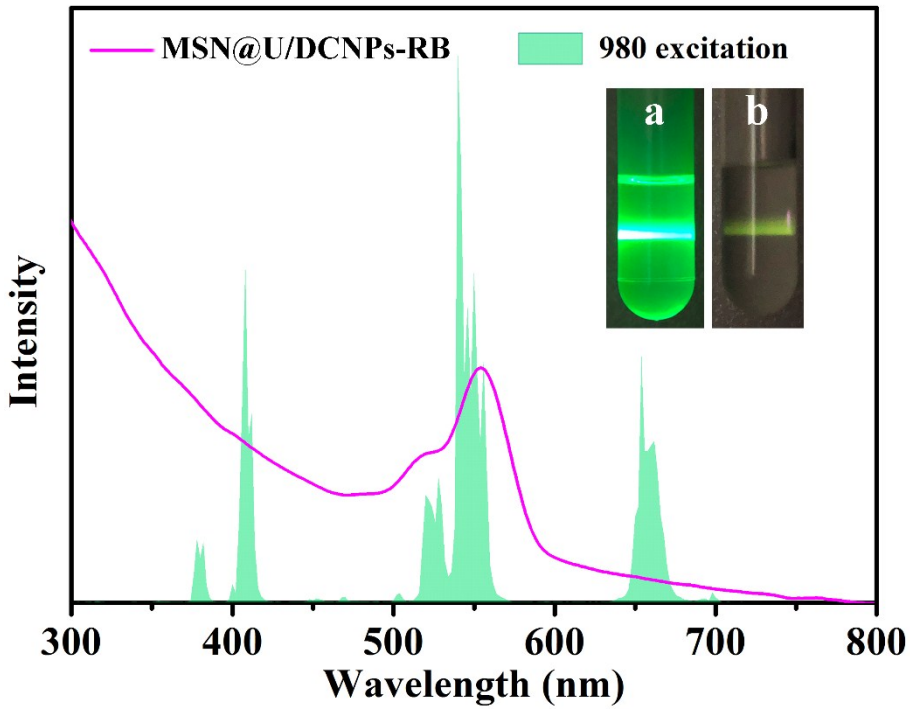

Figure S17. The UV-vis spectra of MSN@U/DCNPs-RB and up-conversion emission spectrum of MSN@U/DCNPs under excitation of 980 nm. The insets represent the luminescence photographs of (a) U/DCNPs in cyclohexane and (b) MSN@U/DCNPs aqueous dispersion under the irradiation of 980 nm laser. It can be seen that the absorption peak of RB is largely consistent with the green upconversion emission of U/DCNPs at 550 nm, ensuring the NIR-activated photodynamic effect.

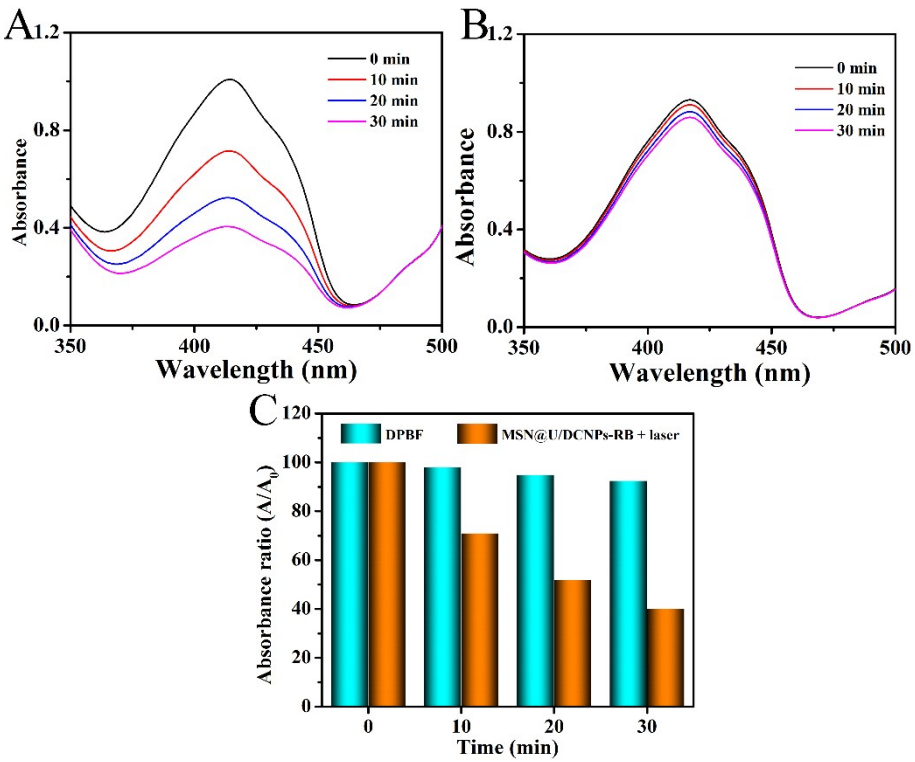

Figure S18. (A) The UV-vis spectra of DPBF solution mixed with MSN@U/DCNPs-RB nanoassemblies after irradiated by 980 nm laser for different time. (B) UV-vis spectra of free DPBF solution exposed to 980 nm laser for different time. (C) The relative intensity of the absorbance of DPBF solution with and without MSN@U/DCNPs-RB nanoassemblies at 420 nm after exposed to 980 nm laser for different time. The maximum absorbance (at 420 nm) of DPBF is clearly decreased upon exposure to 980-nm irradiation, over 60 % of DPBF was degraded by the generated ROS after irradiation for 0.5 h, while the bare NIR irradiation cannot cause the degradation of DPBF.

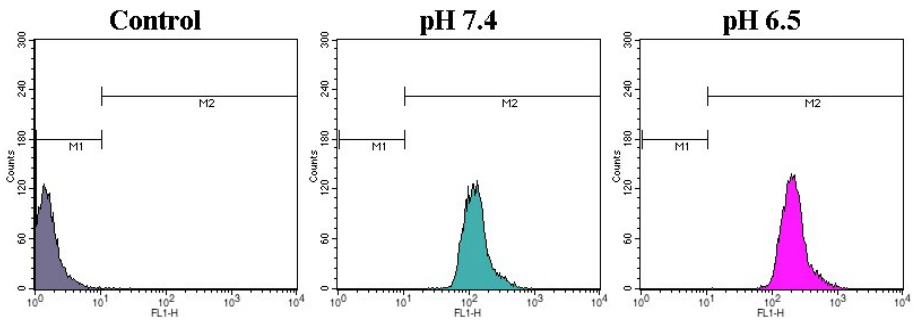

Figure S19. Quantitative analysis of the intensity of the green fluorescence of the cells shown in Figure 4A by flow cytometry. The stronger green fluorescence was observed for the cells treated at pH 6.5 as compared to that at pH 7.4. The quantitative analysis shows that the mean fluorescence in treated cells at pH 6.5 and pH 7.4 were 198.3 and 126.7, respectively, further indicating that the disintegration of the MSN@U/DCNPs nanoassemblies at acidic condition can heighten the intracellular ROS generation ability under NIR irradiation.

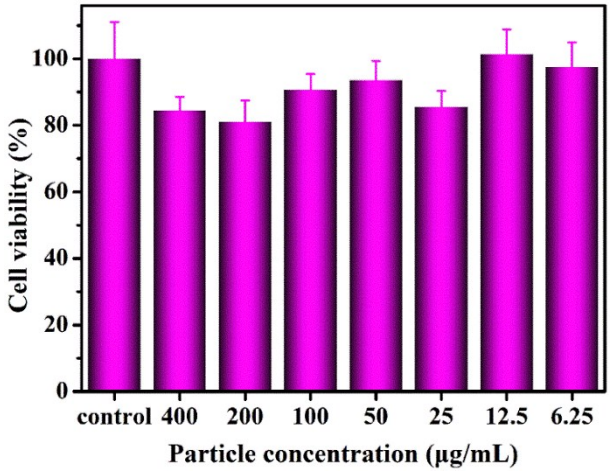

Figure S20. Viability of RAW 264.7 cells incubated with MSN@U/DCNPs for 24 h. The results show that over 80 % cells are alive even exposed to the high concentration of nanoassemblies (400 μg/ml), indicating the low cytotoxicity of the nanoassemblies.

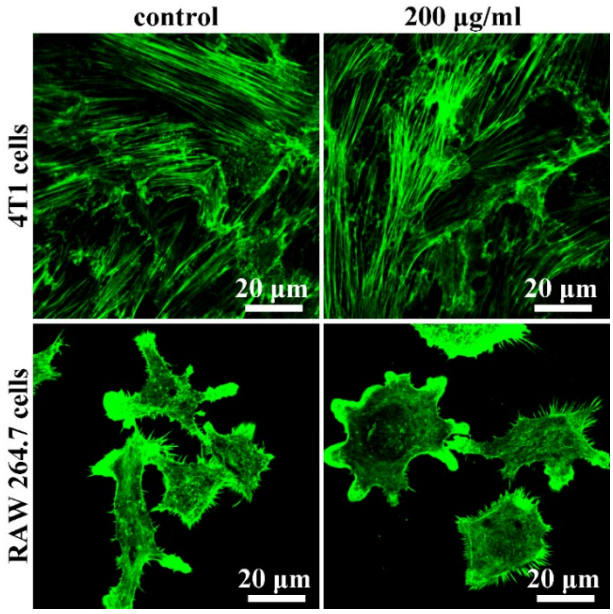

Figure S21. CLSM images of 4T1 and RAW 264.7 cells incubated with MSN@U/DCNPs nanoassemblies (200 μg/mL) for 24 h. The untreated cells were set as control. The cell skeleton was stained with Alexa Fluor 488-conjugated phalloidin. The MSN@U/DCNPs do not show obvious damage on the cell skeleton of 4T1 and RAW 264.7 cells, further indicating the high biocompatibility of the nanoassemblies.

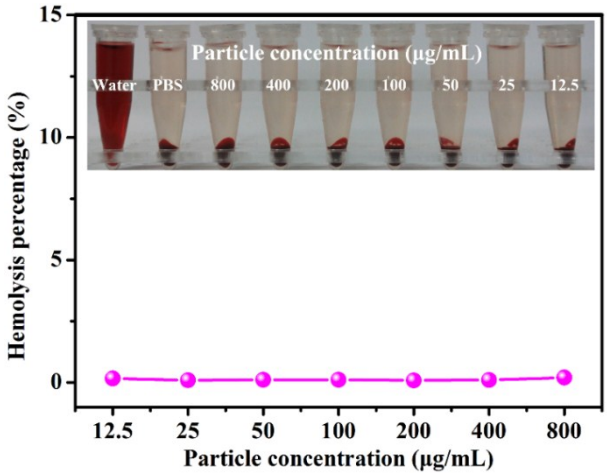

Figure S22. The hemolysis percentage and photographs of red blood cells incubated with MSN@U/DCNPs nanoassemblies for 3 h. The MSN@U/DCNPs nanoassemblies show a very low hemolysis percentage of ~ 0.19 % at the high particle concentration of 800 μg/mL.

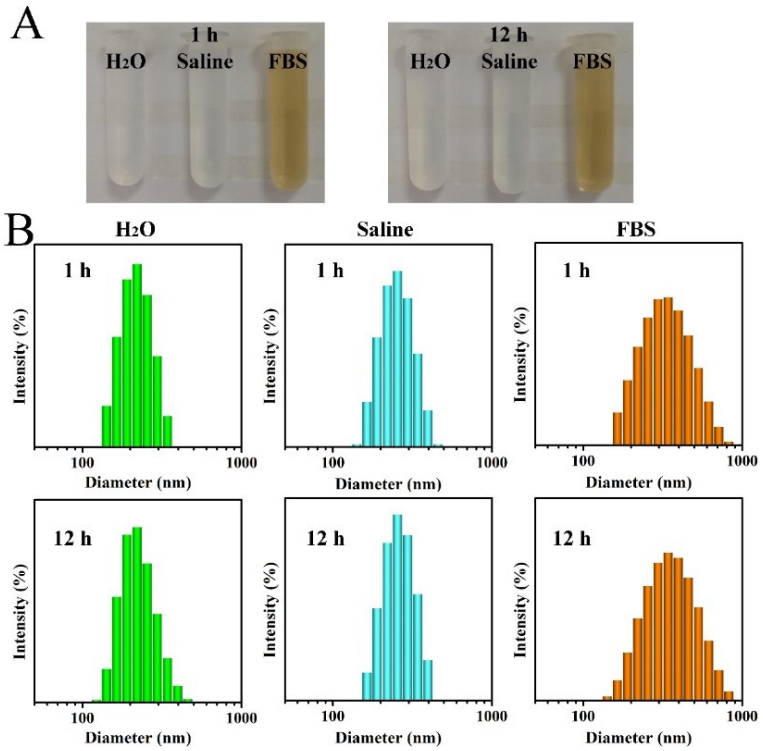

Figure S23. The (A) photographs and (B) size distributions (determined by DLS) of prepared MSN@U/DCNPs nanoassemblies in water, saline, FBS at different periods of times. The solutions maintain clear without observable aggregations after storage in the solutions for 12 h, indicating the good colloid stability of the nanoassemblies, which can also be verified by the consistent size distributions at different time.

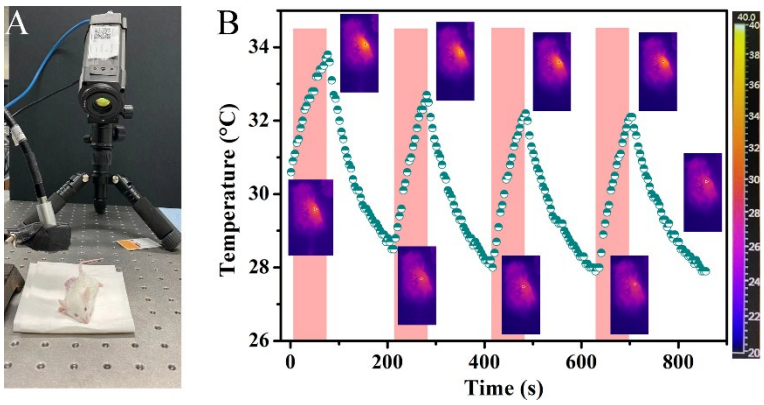

Figure S24. (A) The photograph of thermal imaging setup for monitoring the temperature of tumor site under 980 nm laser irradiation. (B) The temperature variation of tumor site as a function of time under intermittent 980 nm irradiation at 2 W/cm^2 (inset images are the thermal imaging of the mice at corresponding time points during the irradiation process). It can be seen that the increasing of temperature at tumor site is only 3 ~ 4 °C under the intermittent 980 laser irradiation, implying that the intermittent irradiation can minimize the thermal effect on in vivo treatments.

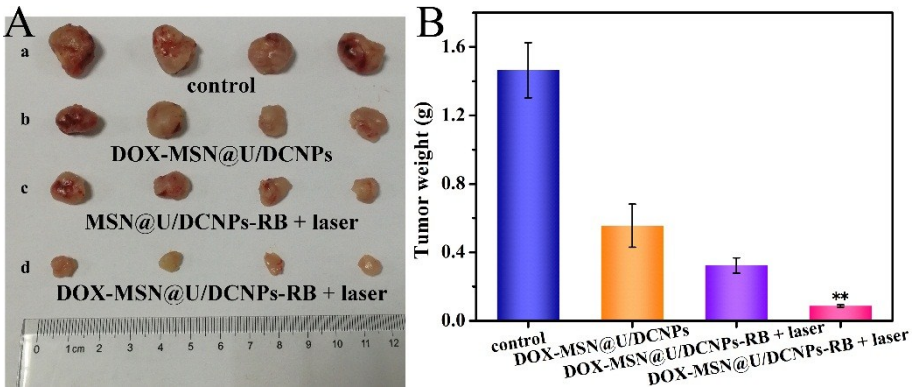

Figure S25. The photographs of excreted tumor after different treatments for 16 days: a) control, b) DOX-MSN@U/DCNPs, c) MSN@U/DCNPs-RB + laser (2 W/cm^2, 20 min) and d) DOX-MSN@U/DCNPs-RB + laser (2 W/cm^2, 20 min). (e) The weight of excreted tumor after different treatments. Compared with groups a, b and c, the tumor growth was significantly suppressed when the chemo- and photodynamic therapies are combined together (group d).

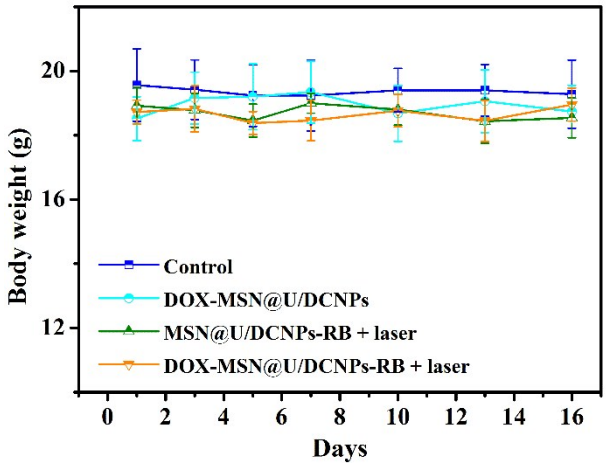

Figure S26. The body weight variation of experimental mice in the treatment duration. No remarkable body weight fluctuation is observed, indicating the good tolerance of the implemented treatment, the good biocompatibility and negligible toxicity of drug-loaded nanoassemblies.

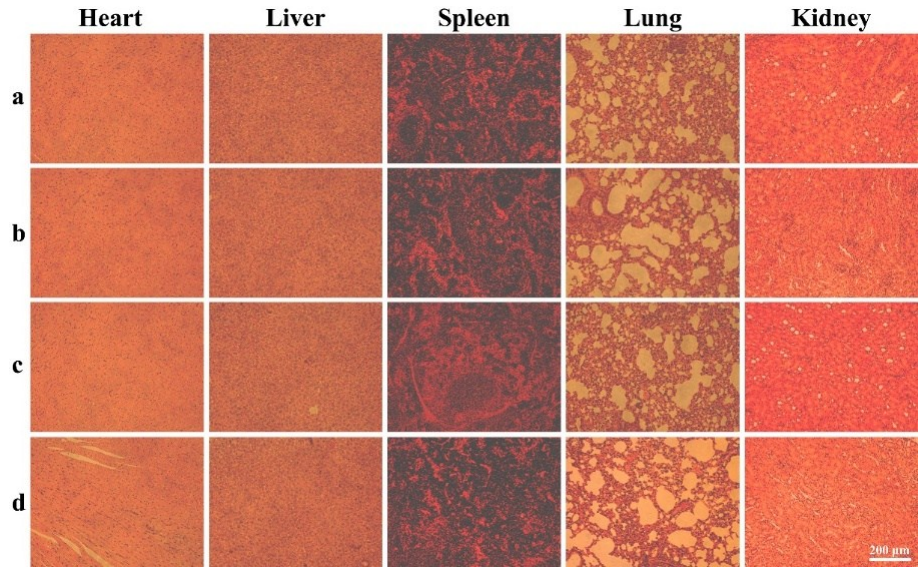

Figure S27. The H&E stained organ slice of mice after different treatments: a) control, b) DOX-MSN@U/DCNPs, c) MSN@U/DCNPs-RB + laser and d) DOX-MSN@U/DCNPs-RB + laser. No remarkable tissue damage or any other side effect was observed on heart, liver, spleen, lung, kidney, thus demonstrated that the treatments were well-tolerated by mice.